Nanomed J. 12(2): 216-225, Spring 2025

RESEARCH PAPER

Conductive composite nanoscaffold of polyurethane/rGO as skin regeneration agent animal model

*Niloufar MolayeeAsl [1, 2], Mahmood Araghi [3], Sayed Habib Kazemi [4], Seyed Hojat Hosseini [5, 6], Samad Nadri [7, 6, 2]**

[1]Student Research Committee, School of Medicine, Zanjan University of Medical Sciences, Zanjan, Iran
[2]Department of Medical Nanotechnology, School of Medicine, Zanjan University of Medical Sciences, Zanjan, Iran
[3]Department of Pathology, School of Medicine, Zanjan University of Medical Sciences, Zanjan, Iran
[4]Department of Chemistry, Institute for Advanced Studies in Basic Sciences (IASBS), Zanjan 45137-66731, Iran
[5]Department of Physiology, School of Medicine, Zanjan University of Medical Sciences, Zanjan, Iran
[6]Zanjan Metabolic Diseases Research Center, Health and Metabolic Diseases Research Institute, Zanjan University of Medical Sciences, Zanjan, Iran
[7]Zanjan Pharmaceutical Nanotechnology Research Center, Zanjan University of Medical Sciences, Zanjan, Iran

ABSTRACT

Objective(s): Traditional wound dressings primarily promote passive wound healing and infrequently promote active wound healing by influencing skin cell. It is known that electrical stimulation (ES) can control the actions of skin cells. In the present study, the conductive electrospun PU/rGO was designed and fabricated and its qualities as skin wound dressings in animal models were examined.

Materials and Methods: In this study, nanocomposite PU (polyurethane)/rGO (reduce graphene oxide) was synthesized using an electrospinning process, investigated via scanning electron microscopy (SEM), transmission electron microscopy (TEM), Fourier transform infrared spectroscopy (FTIR), water contact angle, degradation studies, electrochemical impedance spectroscopy (EIS), bactericidal efficacy, hemolysis and MTT assay. Then, the scaffolds were grafted in full-thickness wounds of animal rats and evaluated by wound closure and histological.

Results: The results showed that the PU/rGO scaffold exhibited antibacterial activity in comparison with PU scaffold and viability showed a notable improvement in cell promotion. In the histopathological analysis, improved dermis development and collagen deposition at the healed wound area of the PU/rGO scaffold with electrical stimulation in comparison to other groups were observed.

Conclusion: A PU/rGO scaffold with electrical stimulation could be an appropriate option for skin tissue engineering and wound healing.

Keywords: *Composite, Electrical stimulation, Scaffold, Tissue engineering, Wound healing*

How to cite this article

MolayeeAsl N, Araghi M, Kazemi SH, Hosseini SH, Nadri S. Conductive composite nanoscaffold of polyurethane/rGO as skin regeneration agent animal model . Nanomed J. 2025; 12(2):216-225. DOI: 10.22038/nmj.2024.78623.1922

INTRODUCTION

Surgical wounds and diabetic ulcers are the most expensive to treat, and range of wounds from $28.1 to $96.8 billion, including costs for infection management [1]. Due to the effect of wounds, therapists, and wound care experts aim to identify novel method therapies for wound healing [2]. Wound healing is a physiological process that is influenced by a number of factors and can be sped up by using appropriate wound care products [3]. Hemorrhage, inflammation, proliferation, and remodeling are the four stages of the wound-healing process [4]. The optimal structures for wound dressing scaffolds should currently contain a number of feature highlights, such as suitable mechanical effects, biocompatibility, pain relief, antibacterial properties, and blood compatibility [5].

Earlier studies have proven that electrical stimulation (ES) is secure for patients [6]. ES is a type of physical therapy in which electrodes are used to administer a low-level electrical current to the target area [7]. ES can elevate healing of acute wounds diabetic ulcers [8], pressure ulcers [9],

* *Corresponding author Emails: nadrisamad@gmail.com; nadri_s@zums.ac.ir*

Note. This manuscript was submitted on March 9, 2024; approved on July 10, 2024

and venous ulcers [10, 11]. It has been suggested that ES could speed up wound healing, increase cellular immunity, and decrease infection [12]. A conductive scaffold might be a supporting structure that mimics the extracellular matrix (ECM) and has capability to stimulate cells and tissues.

Polyurethane is more thrombo-resistant than other polymers and has good mechanical properties, but they have poor electroconductivity, which makes it difficult to stimulate cells or tissue grown on biomaterials [13]. To mask this shortcoming utilizing graphene base material like graphite, graphene, and reduced graphene oxide (rGO) owing to high thermal conductivity, low coefficient of thermal expansion, and good self-lubricant properties were frequently used for various biomedical applications such as electrical stimulation of tissue and cell [14, 15].

In the present study, the conductive electrospun PU/rGO was designed, fabricated, and its responsiveness to electricity and examination of its qualities as skin wound dressings in animal model were observed.

MATERIALS AND METHODS

Fabrication of scaffold

1.1 g Polyurethane (PU) (Sigma-Aldrich, Steinheim, Germany) and rGO (0.3 wt/V%, Sigma-Aldrich) were solved in dimethylformamide (DMF) solvent and mixed together. The fibrous scaffold was made using electrospinning machines under the subsequent condition: high-voltage, 24 kV; flow rate, 0.2 ml/hr; distance, 120 cm; high speed rotating disk, 2,500 rpm.

Nanofiber characterization

The morphology of gold sputter-coated electrospun PU/rGO and PU nanofibers were observed with a scanning electron microscope (SEM). The diameter of the nanofibers was measured from the SEM micrographs using image analysis software. Also, the PU and rGO scattering within the fibrous was estimated using Transmitting electron microscopy (TEM) (Zeiss - EM10C - 100 KV). The sample was prepared by its directly aggregation on a copper grid. Furthermore, Fourier transform infrared (FT-IR) spectroscopy was used to identify the presence of components in the blend. Samples with the same dimensions were crushed and mixed with KBr to make disc. The chemical properties of the PU/rGO scaffold were studied by the FT-IR utilizing Vector 22 Bruker instrument (LabX, Texas).

Electrochemical impedance spectroscopy

An electrochemical impedance spectroscopy (EIS) method was used to check the conductivity of the films. Two sorts of films (PU and PU-rGo) were separately studied in $K_3Fe(CN_5)_3$ solution. Initially, the electrodes were prepared in a square shape (1 cm x 2 cm) from each scaffold and EIS tests were examined at the open circulate potential (OCP) in the frequency range of 100 KHz to 10 MHz with an AC perturbation signal of 10 mV by Zahner/Zennium Potentiostat-Galvanostat (Germany). To end, the electrical parameters were determined by the complex nonlinear least square method. The conductivity of the scaffolds was compared by calculating the electrochemical series resistance (ESR).

Contact angle

The surface contact angle of the PU/rGO sheet was measured by a goniometer in conjunction with the sessile drop method using a Surface Analysis system (SCA20 Physic Data). Distilled water was used as the testing liquid. Two samples were employed for each test, and the average value was calculated. The contact angle method was used to assess the wettability properties of the nanofibrous scaffold.

Degradation test

Short-term degradation experiments were conducted in various solutions: KOH (5 Molar; pH =13.94), HCl (1 Molar; pH= 3.01), and PBS buffer (pH= 7.4). Round samples (N=3) were cut out of modified PU and PU/rGO scaffolds. Three samples taken from each type of scaffold were stored in the 3 ml of the selected mediums. The degradation process was performed at 37 ºC for 15 days. Before the studies, samples were dried and weighed using a Thermobalance set at 60 ºC. After the degradation process, the samples were rinsed with distilled water, dried, and weighed again. The mass loss of the samples was measured by following Equation (2).

$$M = mi - m0$$
$$m0 \times 100\ \% \quad (2)$$

where M, m0, and mi are mass loss (%), initial mass (g), and mass after degradation process (g).

MTT assay

MTT assay was used to calculate the cellular viability to compare PU/rGO scaffold with) T3T

cell line as a control. After 1, 3, and 5 days, cells were incubated with ml of MTT solution (mg/ml in DMEM without FBS) for 4 hr at 37 °C. The supernatant was removed and DMSO was added. MTT absorbance was measured at 570 nm using a microplate reader.

Hemolysis test

Fresh anticoagulated blood from a human volunteer (5 ml) was added to 2.5 ml of PBS. The diluted blood (0.2 ml) was used for test samples. The mixture temperature was kept at 37 º C for 60 min and then centrifuged at 1500 rpm for 10 min. The supernatant was transferred to a 96-well plate and the absorbance values were read at 578 nm using an ELISA Reader. The mean value was calculated. Positive controls consisted of 0.2 ml diluted blood in 10 ml deionized water while negative controls consisted of 0.2 ml diluted blood in 10 ml FBS. The hemolysis degree was calculated as Equation: Hemolysis% = Dt-Dnc÷Dpt-Dnc×100

where Dt is the absorbance of the sample, Dnc is the absorbance of the negative control, and Dpc is the absorbance of the positive control.

Antibacterial activity

The antibacterial activity of scaffolds (PU and PU/rGO) was evaluated by the Mueller Hinton Agar flat dish diffusion method. The recovered bacteria were scraped into pure normal saline solution and shaken to obtain a homogeneous bacterial suspension. Later, the different bacterial suspensions were evenly applied to new agar dishes with sterile cotton swabs, respectively. The zone of inhibition on the plate surface made by two scaffolds was interpreted as an antibacterial effect and compared to commercial gentamicin (5 µg) antibiotic susceptibility disks placed in the middle of each agar plate and used as the positive control. After 24 hr, the zone of inhibition (ZOI) was estimated by the distance between the outer diameter of the inhibition and the diameter of the scaffolds.

Animal study and electrical stimulation

To evaluate the wound healing capacity of the fabricated nanofibers, a full-thickness excision wound model was made on the dorsal of the male wistar rats and the wounds were treated with dressings and the electrical stimulation (15 min; 0.1 Hz, 2.30 V) for 14 days. The macroscopic changes in the wound area (untreated group, polyurethane scaffold group, polyurethane/rGO scaffold group, polyurethane scaffold+electrical stimulation group, and polyurethane/rGO scaffold+ electrical stimulation group) were recorded on 0, 7, and 14 days. Following 14 days, rats were sacrificed under anesthesia and the wound specimens were harvested for histopathological examination. The samples were fixed in 10% buffered formalin, processed and embedded in paraffin. Then, the samples were cut and stained with hematoxylin-eosin (H&E) and Masson's trichrome (MT) stains.

Tail amputation

The male Sprague Dawley rats (200–250 g) were anesthetized, 50% of the tail tip (three rats were assessed for each sample (Four groups: negative Ctrl cotton pad with pressure, positive Ctrl cotton pad without pressure, PU scaffold, and PU/rGO scaffold)) was cut off by surgical scissors; then, the test material was used to fully cover the wound with minimal pressure, and the tail remaining kept naturally bleeding for 15 sec. The blood loss on the scaffold was weighted during the hemostatic process; all manipulations were completed under aseptic conditions.

Statistical analysis

The data were reported as the mean and standard deviation (SD), and the findings were statistically evaluated using Prism 8 version's Student's t-test. Statistics were considered significant for P values

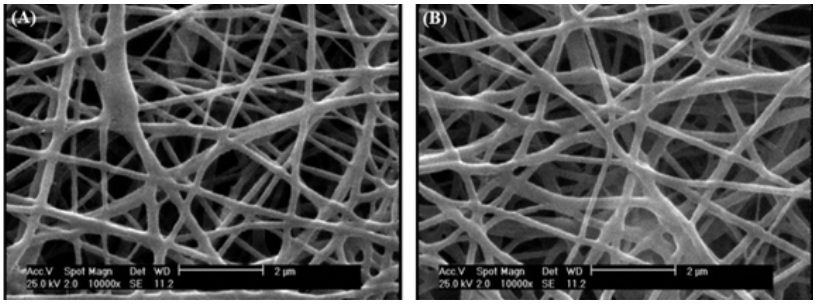

Fig. 1. SEM images of (A) PU/rGO nanofibers and (B) PU nanofiber

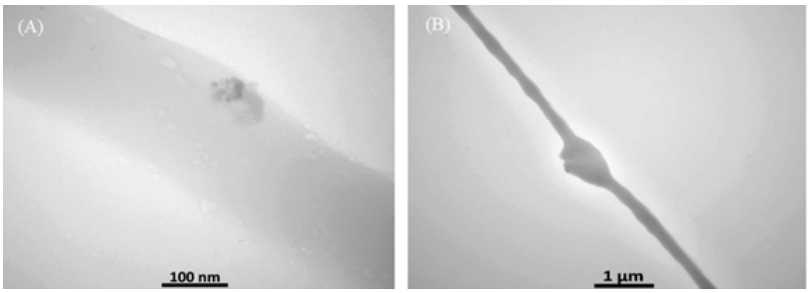

Fig. 2. TEM images of (A) PU/rGO nanofibers and (B) PU nanofibers. The rGO demonstrate by black arrow

under 0.05. Values are naturally expressed as mean ± standard error unless otherwise noted.

RESULTS

Nanofiber characterization

To fabricate an appropriate scaffold for skin tissue engineering, PU/rGO was used in the current study. Morphology and surface properties of electrospun PU and PU/rGo scaffold were determined by SEM, and the micrograph photographs were uniform, smooth, and bead-free nanofibers (Fig. 1A, B). Fig. 1 indicates the fiber diameter distribution, where the average diameter of nanofibers is 193.9 nm for the polyurethane scaffold and 177.7 nm for PU/rGO scaffold. The TEM image confirmed the incorporation of the manufacture of rGO nanoparticles in the PU scaffold. The TEM image related to the PU scaffold has a smooth and fine appearance while the PU-rGo has a rough and wavey pattern due to the incorporation of rGO indicated by a black arrow in Fig. 2 A, B. FTIR graphs (Fig. 3A-B) show the presence of absorption peaks at 1426.26 cm^{-1} (O-H bending), 1577.14 cm^{-1}, and 3427.74 cm^{-1} (N-H stretching) for pure polyurethane and 1575.35 cm^{-1}, 1420.67 cm^{-1} (O-H bending), and 3421.72 cm^{-1} (N-H stretching) for PU/rGO.

Scaffold conductivity

EIS method was used to determine the scaffolds conductivity. The ESR for PU and PU/rGO scaffolds was respectively 10- and 5- ohms (Fig. 4).

Water contact angle measurement

As shown in Fig. 5, the surface hydrophobicity of electro spun PU scaffolds increased by adding

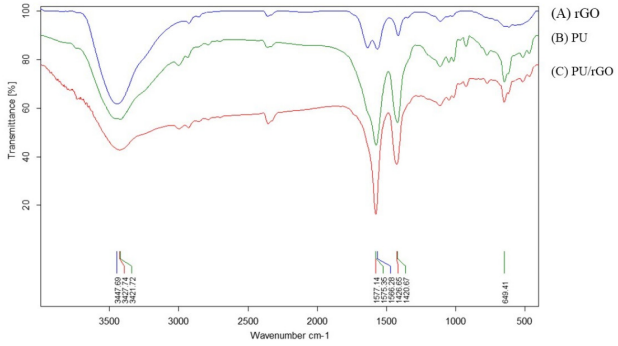

Fig. 3. FTIR spectra of (A) rGO, (B) PU/rGO scaffold, and (C) PU polymer scaffold

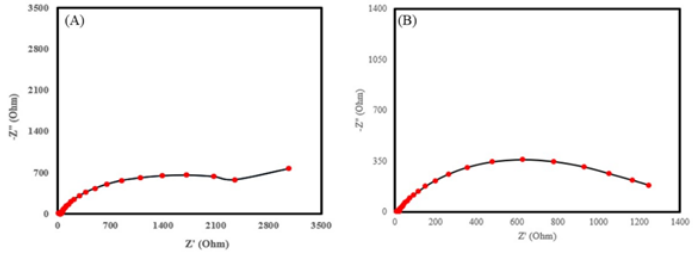

Fig. 4. The EIS spectrums of (A) PU and (B) PU-rGO. The corrected ESR was almost 10 Ω and 5 Ω for polyurethane and polyurethane/rGO, respectively

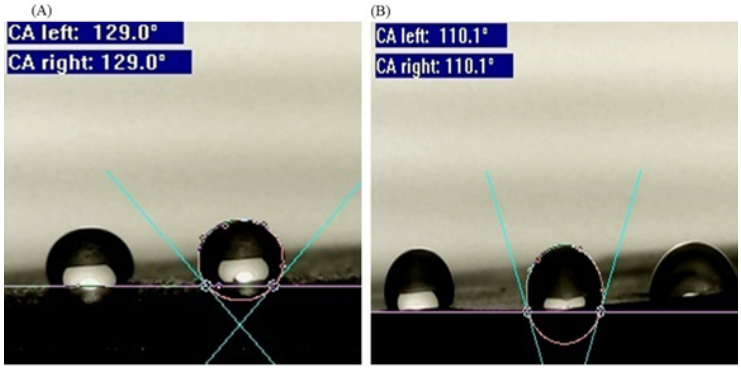

Fig. 5. Contact angle images of (A) PU/rGO nanofibers and (B) PU nanofiber

rGO owing to its hydrophobicity nature and positive surface charge. Overall, both composites are hydrophobic according to the results.

Degradation test

In three different settings, scaffolds behaved differently, and in an alkaline solution, they degrade the most quickly, in the PBS solution didn't lose weight, and appeared to have a minor change in weight when exposed to the acidic solution. The results showed the most degradation in a basic solution, the least degradation in an acidic solution, and no degradation in a neutral solution (Table 1, Supplementary Fig. 1).

Table 1. The mass loss of scaffold (mg).

Scaffold	1 M HCl	PBS	5M KOH
PU	13 %	0	46.6 %
PU/rGO	0	0	25.8 %

MTT assay

For the purpose of calculating the proliferation of cells on constructed scaffolds, a cytocompatibility assay is essential. We saw an increase in the growth of cultured cells on the rGO/PU scaffold in the different days (1, 3, and 5). On the 5th day, there was a significant difference in the growth rate of the cultured cells on the scaffold compared to the control (cell culture plate) (Fig. 6).

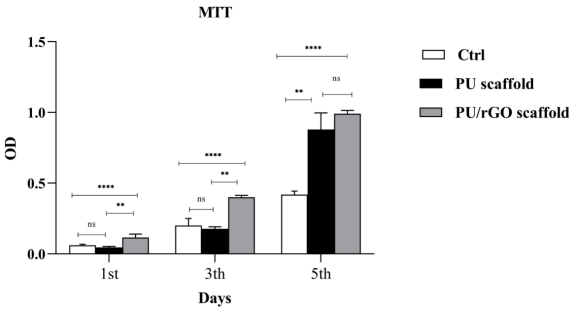

Fig. 6. The cytotoxicity evaluation of scaffold in the different culture times by MTT assay

Hemolysis test

The blood compatibility of the materials is closely tied to hemolysis, described as the release of hemoglobin into plasma because of injury to erythrocytes. Fig. 7 displays the results of the experiment on the hemolytic rate. In this study, after anesthetizing the rats, half of their tails were amputated and the treatments were performed. Blood coagulation time was recorded between 9 and 6 min between the groups with scaffolds. After the tail amputation, the average weight of the scaffolds in the positive control, the negative

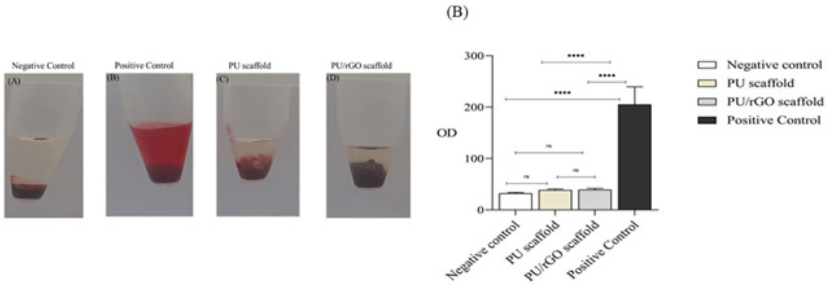

Fig. 7. Hemolysis rate test of (A) negative control (PBS), (B) the positive control (Distilled water)), (C) PU scaffold, and (D) PU/rGO scaffold

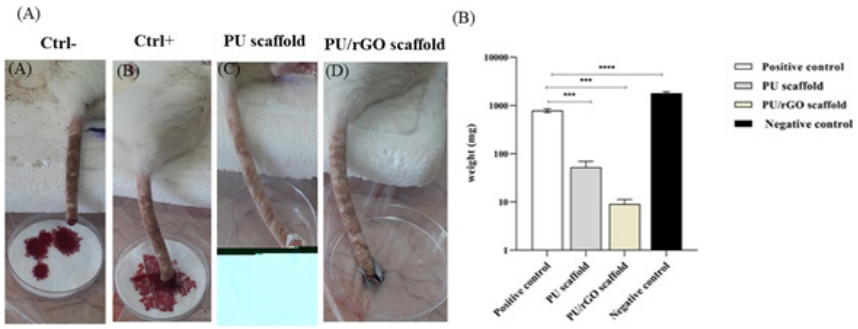

Fig. 8. Hemostasis in rat tail amputation. (a) Schematic diagram of rat tail amputation. (b) blood loss in the rat tail amputation model. Picture of hemostasis with each material ((A) ctrl- cotton pad with pressure, (B) ctrl+ cotton pad without pressure, (C) PU scaffold, (D) PU/rGO scaffold)

control, the PU scaffold, and PU/rGO scaffold was 786, 1801, 37.2, and 9.54, respectively (Fig. 8).

Antibacterial activity

The antibacterial effect of scaffolds was examined through disc diffusion assay. The results showed that there was the absence of the zone of inhibition (ZOI) in the PU scaffold in Fig. 9 (a-b). The best ZOI was in the PU/rGO scaffold. The rGO scaffold against *S. aureus* and *E. coli* was 20.3 mm and 19.21 mm, respectively. Additionally, gentamicin's disc antibiogram against *S. aureus* and *E. coli* was 20.24 mm and 21.14 mm (Table 2).

Wound closer

In vivo full-thickness wound healing study was created with full-thickness on the dorsal side of rats, analyzed for 14 days, and the closing of the wound closure was measured on days 0, 7, and 14. The results show that when the rats were treated with PU/rGO scaffolds + electrical stimulation and PU + electrical stimulation, a significant wound closure rate was observed compared to others. Furthermore, when they were treated with PU and PU/rGO scaffolds without electrical stimulation, increased rate of wound closure was documented compared to the rats without treatment (Fig. 10).

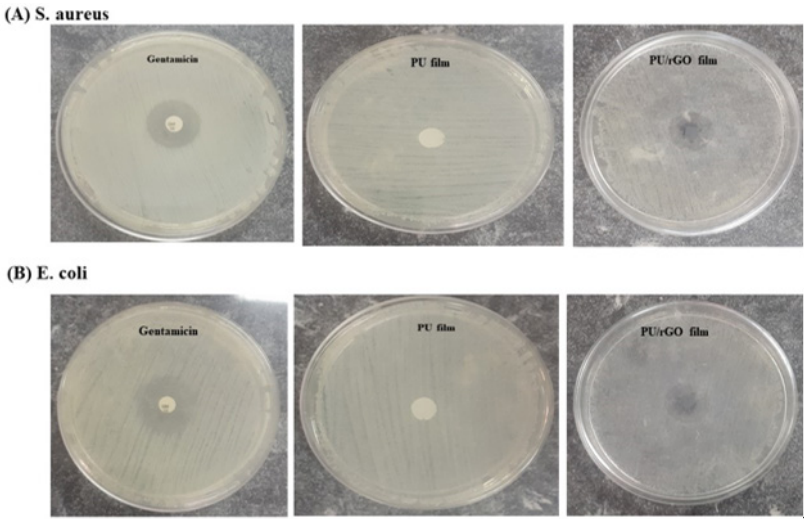

Fig. 9. Antibacterial activity on (A) Gram-positive *Staphylococcus aureus* and (B) Gram-negative *Escherichia coli*

Table 2. Zone of inhibition in the strains studied (mm)

Microorganisms	PU scaffold	Positive control	Pu/rGO scaffold
Staphylococcus aureus	0	20.24	20.3
Escherichia coli	0	21.14	19.21

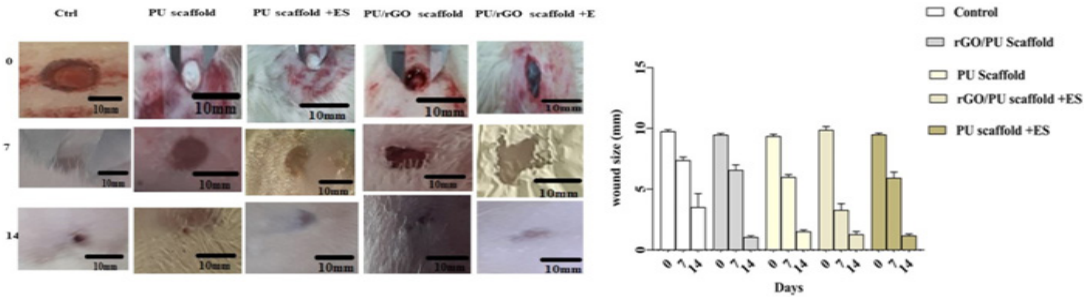

Fig. 10. Wound kinetics of large wounds on various days during healing process (Scale bar = 10 mm)

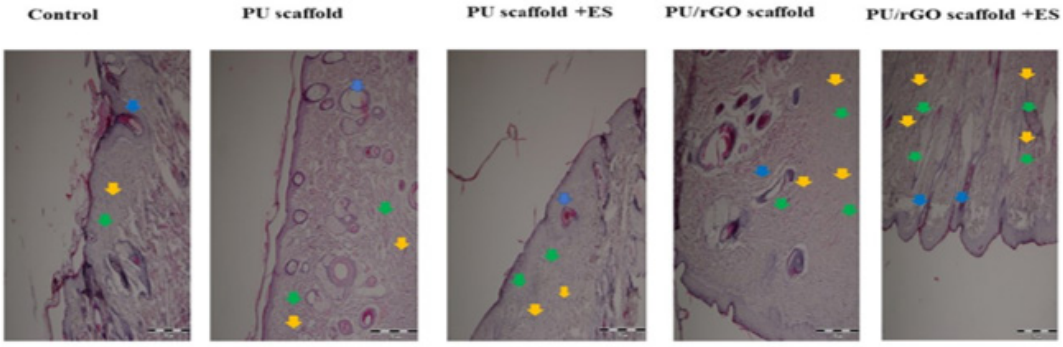

Fig. 11. H&E staining. Images of fibroblast cells (green arrow), collagen (orange arrow), and hair follicles (blue arrow) from the dorsal of the rats (scale bar 200 µm)

Histological analysis

As well H&E staining in PU/rGO and PU+ES scaffolds with electrical stimulation, compared to the other groups without electrical stimulation, showed an increase in the thickness of granulation tissue, lack of inflammation, and angiogenesis (Fig. 11).

MT staining indicated that when using ES with PU/rGO and PU scaffolds, the rate of collagen deposition is higher than scaffold without ES (Fig. 12).

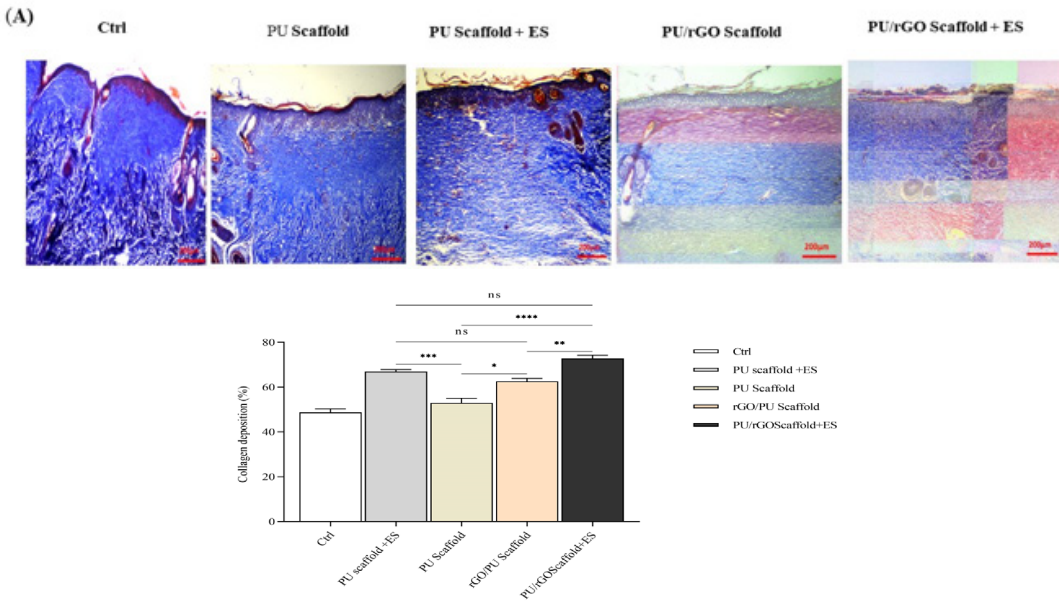

Fig. 12. Masson's Trichrome Staining of Day 14 wounds; and (B) quantitative collagen deposition. *P< 0.05 compared to the untreated group. (Scale bar: 200 µm)

DISCUSSION

The use of scaffolds in tissue and organ regeneration is highly regarded for repairing various types of body damage, such as skin ulcers. A scaffold serves as a dressing and should allow oxygen to pass through while replicating the skin's extracellular matrix (ECM). Nanocomposite scaffolds are particularly effective because they structurally resemble the body's ECM, providing a conducive environment for cell growth. Research indicates that enhancing blood flow to the wound accelerates wound healing processing. Thus, designing a scaffold that ensures adequate blood supply is a key research challenge in this field.

The present literature was designed to explore the inherent capacity of PU/rGO scaffold and ES to support wound healing in an in vivo rat model.

Electrospinning is favored for creating nanofibrous scaffolds due to its simplicity, affordability, and speed compared to other methods like solvent casting and melt mixing. In this work, a conductive scaffold was developed using electrospinning with polyurethane and rGO, leveraging their biomedical potential. Polyurethane's adaptability, durability, and low-temperature flexibility make it ideal for diverse medical applications. It has rather excellent biocompatibility, mechanical properties, and it is naturally hard resistant to thrombosis than other polymers, and for this purpose, it is considered a suitable polymer for tissue engineering studies [16, 17]. rGO possesses unequaled electronic, thermal, mechanical characteristics, and nanoelectronics, conductive thin films, supercapacitors, nanosensors, and nonbiomedical are such applying. However, in the present study, we created a polyurethane scaffold with rGO by electrospinning method.

The SEM images showed the production of nanofibers without bead, smooth, and uniform with the minimum average diameter (177.7 nm) of the fibers. TEM examination revealed that rGO was spread homogeneously within the nanofibers, impacting the conductivity of the entire nanofiber. To determine the molecular nature of the fabricated scaffold, FTIR spectra was appplied; the presence of absorption peaks at 1575 cm^{-1} and 1420 cm^{-1} related to polyurethane scaffold and peaks at 1577 cm^{-1} and 1426 cm^{-1} related to rGO scaffold, and the functional groups proved present in these scaffolds. Totally, all the mentioned results, clearly demonstrate that rGO successfully bonded to the surface of polyurethane nanosheets [18].

As mentioned, the aim of this study is to raise the conductivity of polyurethane polymer by adding rGO structure for use in skin tissue engineering. According to an earlier study raising the conductivity of the scaffold by adding a suitable conductive material could result in a fine fiber diameter. In this report, nanostructures were made with a polyurethane polymer substrate during the electrospinning process, in which rGO nanoparticles were dispersed. The other study used the electrospinning method; the base polymer of polyurethane/cellulose acetate contained rGO/Ag was applied to this scaffold for wound healing. In the current paper, we used EIS technique to investigate the conductivity of the PU/rGO scaffold and compare it with the PU scaffold as a control sample. The addition of rGO nanoparticles to the scaffold structure led to an increase in the load transfer resistance of the whole system. rGO is a superconducting nanoparticle, known for its excellent mechanical and electrical properties; so it can significantly increase the conductivity of composites [19].

To use a scaffold as a wound dressing, it is required to perform hydrophobicity and degradability tests to properly analyze the amount and time of destruction in the different conditions. The results of the contact angle obtained in both polymers with numbers of 124º and 119º for rGO/PU and PU scaffolds, respectively, indicate the hydrophobic nature of both scaffolds. Long et al. reported the hydrophobic scaffold could not adhere to the wound area, also prevent bleeding, thus avoiding secondary bleeding, and declining the inflammation [20]. Yu et al. developed asymmetric super hydrophobicity wound dressing with bacterial adhesion property and subsequently decreasing inflammation of the wound [21]. It is assumed adsorption of blood proteins onto the hydrophobic structure leads to alterations in the protein structure, these processes may expose protein epitopes thereby speeding up the activation of an immune response through recognition by inflammatory cells [22, 23]. Hydrophobic scaffolds exhibit an increased susceptibility to microbial colonization, including the formation of biofilms, which hinders the natural healing process [24-26].

So as to use a scaffold as a wound dressing, it is necessary to perform degradability tests to properly analyze the amount and time of

destruction in different conditions. In this survey, the short-term degradation test of mass loss of the both scaffolds (PU and rGO/PU) showed that the highest and lowest percentage of loss weight was in the basic solution and acidic medium, respectively.

One of the most meaningful cases in the study of nanobiotechnology is to investigate their toxicity on cells, which should be considered in the studies. The results of the MTT assay indicate the non-toxicity of scaffold on proliferation of cells. In the present work, the hemolysis named as the release of hemoglobin in the plasma due to red blood cell damage and related to the blood adjustment substance, was reviewed. The hemolysis rate of all samples in the laboratory conditions was lower than that of the positive control sample, which indicates the negative impact of the scaffold on red blood cells. However, due to the presence of functional groups numerous oxygen, the rGO nanosheets activate platelets and then irritate their strong aggregation reaction.

Since bacterial infection is the primary cause of wound infection, it is important to assess the antibacterial activity of wound dressing before using it to treat wounds. Thereby, the antibacterial properties of scaffolds were evaluated against Gram-negative *E. coli* and Gram-positive Staphylococcus aureus. Graphene-based material has rough edges that causes physical harm to bacterial membranes, which is what causes the material's antibacterial properties to work. These findings determined that the antibacterial efficiency of fabricated scaffold is appropriate.

In present study, our group increased the conductivity of the scaffold by adding rGO to the scaffold structure and investigated its potential effect on the wound healing process. Histological studies show the synergy effect of the scaffold and ES on collagen formation and that the application of electrical current and synthesized scaffolding type has a positive effect on wound healing. H&E staining displays the lowest levels of inflammation and the highest amount of granulation and epithelialization in the scaffolding group by applying the electric current. However, the previous study reported that low concentrations of rGO stimulated the synthesis of intracellular reactive oxygen species and reactive nitrogen species to induce angiogenesis [27]. In a similar study, researchers confirmed the function of rGO in collagen synthesis, angiogenesis, inflammation reduction, and re-epithelialization [28]. In another study, the fabricated carboxymethyl guargum/rGO /PVA scaffold showed production of collagen on the 14th day of treatment [29].

CONCLUSION

The goal of this study is to combine PU and rGO to create the optimum wound-healing scaffold possible by using the synergy effect of the ES mechanism. After 14 days of the trial, there was a considerable improvement in the granulation tissue thickness, collagen deposition, angiogenesis, and absence of inflammation for wound site healing in rat skin treated with ES and scaffolds.

ACKNOWLEDGMENTS

This work supported by Zanjan University of Medical Sciences (Grant number: A-12-892-37, Ethical Code: IR.ZUMS.REC.1400.389).

CONFLICTS OF INTEREST

None.

REFERENCES

1. Nussbaum SR, Carter MJ, Fife CE, DaVanzo J, Haught R, Nusgart M, et al. An economic evaluation of the impact, cost, and medicare policy implications of chronic nonhealing wounds. Value Health. 2018;21(1):27-32.
2. Heyer K, Protz K, Glaeske G, Augustin M, Herberger K, Goepel L, et al. Effectiveness of advanced versus conventional wound dressings on healing of chronic wounds: systematic review and meta-analysis. Dermatology. 2013;226(2):172-184.
3. Abd El-Hack ME, Alagawany M, Arif M, Chaudhry MT, Emam MA, Patra AK, et al. Antimicrobial and antioxidant properties of chitosan and its derivatives and their applications: a review. Int J Biol Macromol. 2020;164:2726-2744.
4. Saghazadeh S, Rinoldi C, Schot M, Saheb Kashaf S, Sharifi F, Jalilian E, et al. Drug delivery systems and materials for wound healing applications. Adv Drug Deliv Rev. 2018;127:138-166.
5. Nakagami G, Sanada H, Konya C, Kitagawa A, Tadaka E, Tabata K, et al. Effect of vibration on skin blood flow in an *in vivo* microcirculatory model. Biosci Trends. 2007;1(3):161-166.
6. Foulds I, Barker A. Human skin battery potentials and their possible role in wound healing. Br J Dermatol. 1983; 109(5): 515-522.
7. Machado AF, Liebano RE, Helene A, Ferreira LM. Effect of high- and low-frequency transcutaneous electrical nerve stimulation on angiogenesis and myofibroblast proliferation in acute excisional wounds in rat skin. Adv Skin Wound Care. 2016; 29(8): 357-363.
8. Sari Y, Alavi SM, Rahimi M, Ghasemi A, Mohammadi F, et al. A comparative study of the effects of vibration and electrical stimulation therapies on the acceleration of wound healing in diabetic ulcers. J Ners. 2017;12:253-260.
9. Adunsky A, Ohry A. Decubitus direct current treatment (DDCT) of pressure ulcers: results of a randomized double-blinded placebo controlled study. Arch Gerontol Geriatr. 2005;41(3):261-269.

10. Houghton PE, Campbell KE, Fraser CH, Griffin L, Harris C, Keast DH, et al. Electrical stimulation therapy increases rate of healing of pressure ulcers in community-dwelling people with spinal cord injury. Arch Phys Med Rehabil. 2010;91(5):669-678.
11. Szuminsky NJ, Albers AC, Unger P, Eddy J, Harkins D, et al. Effect of narrow, pulsed high voltages on bacterial viability. Phys Ther. 1994;74(7):660-667.
12. Yeganeh H, Ghaffari A, Mehdipour-Ataei S, Mohammadi A, et al. Synthesis, characterization and preliminary investigation of blood compatibility of novel epoxy-modified polyurethane networks. J Bioact Compat Polym. 2008;23(3):276-300.
13. Moghadam AD, Omrani E, Menezes PL, Rohatgi PK, et al. Mechanical and tribological properties of self-lubricating metal matrix nanocomposites reinforced by carbon nanotubes (CNTs) and graphene–a review. Compos Part B Eng. 2015;77:402-420.
14. Gautam R, Kumar S, Singh R, Singh H, et al. Dry sliding wear behavior of hot forged and annealed Cu–Cr–graphite in-situ composites. Wear. 2011;271(5-6):658-664.
15. Hernández HH, Cordero IA, Martínez VG, López AL, Pérez JS, Gómez MS, et al. Electrochemical impedance spectroscopy (EIS): a review study of basic aspects of the corrosion mechanism applied to steels. Electrochem Impedance Spectrosc. 2020;12(3):137-144.
16. Patient JD, Smith AB, Johnson CD, Brown EF, Davis GH, Wilson IJ, et al. Nanofibrous scaffolds support a 3D *in vitro* permeability model of the human intestinal epithelium. Front Pharmacol. 2019; 10:456.
17. Sari Y, Sutrisna E. The effect of short duration of electrical stimulation on wound healing in acute wound in a rat model. Wound Med. 2019;24(1):36-44.
18. Bian J, Wang L, Zhang M, Li Q, Chen Y, Liu H, et al. Bacteria-engineered porous sponge for hemostasis and vascularization. J Nanobiotechnol. 2022;20(1):47.
19. Tu Y, Li X, Zhang Z, Wang H, Liu J, Chen Y, et al. Destructive extraction of phospholipids from Escherichia coli membranes by graphene nanosheets. Nat Nanotechnol. 2013;8(8):594-601.
20. Bahrami S, Solouk A, Mirzadeh H, Seifalian AM. Electroconductive polyurethane/graphene nanocomposite for biomedical applications. Compos Part B Eng. 2019;168:421-431.
21. S Członka, A Strąkowska, K Strzelec, A Kairytė, A Kremensas. Bio-based polyurethane composite foams with improved mechanical, thermal, and antibacterial properties. Mater. 2020;13(5):1108.
22. Hong JH, Lee JH, Kim SH, Park JS, Kim YH, Lee YS, et al. Electrospinning of polyurethane/organically modified montmorillonite nanocomposites. J Polym Sci B Polym Phys. 2005;43(22):3171-3177.
23. Lan M, Zhang Y, Li X, Wang J, Chen H, Liu Q, et al. Hierarchical polyurethane/RGO/BiOI fiber composite as flexible, self-supporting and recyclable photocatalysts for RhB degradation under visible light. J Ind Eng Chem. 2022;108:109-117.
24. Long C, Zhang Y, Li X, Wang J, Chen H, Liu Q, et al. Asymmetric composite wound nanodressing with superhydrophilic/superhydrophobic alternate pattern for reducing blood loss and adhesion. Compos B Eng. 2021;223:109134.
25. Yu B, Zhang Y, Li X, Wang J, Chen H, Liu Q, et al. Asymmetric wettable composite wound dressing prepared by electrospinning with bioinspired micropatterning enhances diabetic wound healing. ACS Appl Bio Mater. 2020;3(8):5383-5394.
26. Collier T, Anderson J. Protein and surface effects on monocyte and macrophage adhesion, maturation, and survival. J Biomed Mater Res. 2002;60(3):487-496.
27. Tang L, Thevenot P, Hu W. Surface chemistry influences implant biocompatibility. Curr Top Med Chem. 2008;8(4):270-280.
28. Han G, Ceilley R. Chronic wound healing: a review of current management and treatments. Adv Ther. 2017;34(3):599-610.
29. Guo S, DiPietro LA. Factors affecting wound healing. J Dent Res. 2010;89(3):219-229.
30. LC Gomes, LN Silva, M Simões, LF Melo, FJ Mergulhão. Escherichia coli adhesion, biofilm development and antibiotic susceptibility on biomedical materials. J Biomed Mater Res A. 2015;103(4):1414–23.
31. I Miescher, J Rieber, TA Schweizer, M Orlietti, A Tarnutzer, F Andreoni, et al.*In vitro* assessment of bacterial adhesion and biofilm formation on novel bioactive, biodegradable electrospun fiber meshes intended to support tendon rupture repair. ACS Appl Mater Interfaces. 2024;16(5):6348-6355.
32. Iga C, Ohtsuki C, Fukuda M, Yoshikawa M, Takemura A, Shimizu Y, et al. Polyurethane composite scaffolds modified with the mixture of gelatin and hydroxyapatite characterized by improved calcium deposition. Polymers. 2020;12(2):410.
33. Balaji A, Zhang J. Electrochemical and optical biosensors for early-stage cancer diagnosis by using graphene and graphene oxide. Cancer Nanotechnol. 2017;8(1):100-115.
34. Thangavel P, Kannan R, Ramachandran B, Moorthy G, Suguna L, Muthuvijayan V, et al. Development of reduced graphene oxide (rGO)-isabgol nanocomposite dressings for enhanced vascularization and accelerated wound healing in normal and diabetic rats. J Colloid Interface Sci. 2018; 517:251-264.
35. Koyyada A, Orsu P. Nanofibrous scaffolds of carboxymethyl guargum potentiated with reduced graphene oxide for *in vitro* and *in vivo* wound healing applications. Int J Pharm. 2021;607:121035.